

# Higgs portal vector dark matter interpretation: review of Effective Field Theory approach and ultraviolet complete models

Mohamed Zaazoua<sup>1</sup>, Loan Truong<sup>2</sup>, Kétévi A. Assamagan<sup>3</sup>, and Farida Fassi<sup>1</sup>

<sup>1</sup>Mohammed V University in Rabat, Faculty of Science

<sup>2</sup>University of Johannesburg, Department of Mechanical Engineering Science

<sup>3</sup>Brookhaven National Laboratory (BNL)

December 29, 2021

A description of the Higgs portal-vector dark matter interpretation of the spin-independent dark-matter nucleon elastic scattering cross section using the invisible Higgs decay width measured at the LHC is presented. The usage of Effective Field Theory approach and ultraviolet complete models is discussed. The inclusion of these theoretical scenarios in LHC public results in comparison with direct detection results is proposed. Dark matter in the sub-GeV mass range is additionally discussed.

## 1 Introduction

The existence of a Dark Matter (DM) component of the universe is now firmly established, receiving astrophysical observations [1] showing strong evidence that dark matter exists. While the nature of the DM particles and their interactions remains an open question, it is clear that the viable candidates must lie in theories beyond the Standard Model (BSM). A particularly interesting class of candidates are weakly interacting massive particles (WIMP). They appear naturally in many BSM theories. Due to their weak-scale interaction cross-section, they can accurately reproduce the observed DM abundance in the Universe today[2].

At the LHC, experiments can explore Higgs portal scenarios in which the 125 GeV Higgs boson can achieve substantial coupling with WIMP candidates (such as singlet scalar  $S$ , vector  $V$ , fermion  $\chi$ ) thus inducing interaction between WIMP and nucleon while WIMP could be Higgs' invisible decay products [3–16]. Therefore, limits on the branching ratio ( $\mathcal{B}_{H \rightarrow \text{inv}}$ ) from invisible Higgs decay can be used to interpret on spin-independent DM-nucleon elastic scattering cross section  $\sigma^{\text{SI}}(\text{WIMP-N})$ . That interpretation can complement and be compared with the direct and indirect DM particle candidate detection results [17–22].

The approach of using Effective Field Theory (EFT) is based on describing the unknown DM interactions with the Standard Model (SM) in a very economical way. This has attracted significant attention, especially because of its simplicity and flexibility which allows it to be used in vastly different search contexts. For the scalar and fermion WIMP candidates, EFT approach [7, 8] can be safely used. Hence, the EFT approach [7] is used in LHC Run-1 papers [23, 24]. Unfortunately, the validity of this approach, as far as vector case has been questioned and the limitations to the use of

EFT has been recognized by the theoretical and experimental communities [25]. The recent efforts to develop more model-independent approaches to DM searches stimulated this literature [26], in which the EFT approach is shown to come from a valid ultraviolet (UV) model and its results are viable. The UV completion models have been investigated in both scenarios: along with the EFT approaches and in a separate model with additional fermions [27].

This note is organized as follows: common notations used in the analyses are presented in Section 2.1. EFT approaches and UV complete models are described and discussed in Sections 2.2; 2.3; 2.4 and 2.5. Section 3 is dedicated to discuss the proposal of the Higgs portal-vector dark matter (VDM) interpretation on the spin-independent dark-matter nucleon elastic scattering cross section using the invisible Higgs decay width. Dark matter in the sub-GeV mass range is presented in Section 4. The note is summarized in Section 5.

## 2 Analysis

### 2.1 Common convention

1.  $h, H$ : 125 GeV Higgs boson.
2.  $v = 246$  GeV: Higgs field's vacuum expectation value.
3.  $m_p = m_N = 0.938$  GeV: proton-nucleon mass.
4.  $m_V = M_V$ : vector boson mass.
5.  $m_h = M_H = m_H = 125$  GeV: Higgs boson mass.
6.  $\beta_V = \sqrt{1 - 4 \frac{m_V^2}{m_h^2}}$
7.  $\beta_{VH} = \sqrt{1 - 4 \frac{m_V^2}{m_h^2}} \left( 1 - 4 \frac{m_V^2}{m_h^2} + 12 \frac{m_V^4}{m_h^4} \right)$
8.  $m_r^2 = \mu_{Vp}^2 = \frac{m_V^2 m_p^2}{m_V^2 + m_p^2}$ : vector DM reduced mass.
9.  $\mathcal{B}_{H \rightarrow \text{inv}}$ : Branching ratio of  $H \rightarrow$  invisible, upper limit at 90% CL of 11% is used as the result from the recently published VBF+MET analysis [28].
10.  $\Gamma^{\text{inv}}(h \rightarrow VV) = \Gamma_{\text{inv}}^H = \mathcal{B}_{H \rightarrow \text{inv}} \Gamma_H^{\text{tot}} = \frac{\mathcal{B}_{H \rightarrow \text{inv}}}{1 - \mathcal{B}_{H \rightarrow \text{inv}}} \Gamma_h^{\text{SM}}$
11.  $\Gamma_h^{\text{SM}} = 0.00407$  GeV: Higgs width at  $m_H = 125$  GeV
12.  $\hbar c = 1.97327 \times 10^{-14}$  GeV  $\times$  cm
13.  $f_N = 0.308(18)$ : Higgs-nucleon form factor [29]

### 2.2 Effective Field Theory approach

In LHC Run-1 papers [23, 24] where  $H \rightarrow$  invisible combination was done, the 90% CL upper limit on  $\mathcal{B}_{H \rightarrow \text{inv}}$  was converted into 90% CL upper limit on  $\sigma^{\text{SI}}(\text{WIMP-N})$  with WIMP being either a scalar, a fermion or a vector boson by using the EFT approach [7]. In the scope of this note, only the VDM interpretation is discussed.

This approach suggests a model-independent Lagrangian for hVV coupling as the following (Equation 1 of Ref. [7]):

$$\mathcal{L}_V = \frac{1}{2}m_V^2 V_\mu V^\mu + \frac{1}{4}\lambda_V(V_\mu V^\mu)^2 + \frac{\lambda_{hVV}}{4}H^\dagger H V_\mu V^\mu. \quad (1)$$

The Lagrangian has only two free parameters: hVV coupling  $\lambda_{hVV}$  and vector mass  $m_V$ . Using this Lagrangian,  $\sigma^{\text{SI}}(\text{V-N})$  together with Higgs invisible decay width  $\Gamma_{\text{inv}}^{\text{H}}$  are derived as functions of  $m_V$  and  $\lambda_{hVV}$  as the following (Equations 4 and 5 of Ref. [7]):

$$\Gamma^{\text{inv}}(h \rightarrow VV) = \lambda_{hVV}^2 \frac{v^2 \beta_V m_h^3}{512 \pi m_V^4} \times \left(1 - 4 \frac{m_V^2}{m_h^2} + 12 \frac{m_V^4}{m_h^4}\right) \quad (2)$$

$$\sigma^{\text{SI}}(\text{V-N}) = \lambda_{hVV}^2 \frac{m_N^2 f_N^2}{16 \pi m_h^4 (m_V + m_N)^2} \quad (3)$$

Extracting the coupling  $\lambda_{hVV}$  from Equation 2 and substitute into Equation 3, one can find a direct relation between  $\sigma^{\text{SI}}(\text{V-N})$  and  $\Gamma_{\text{inv}}^{\text{H}}$ :

$$\begin{aligned} \lambda_{hVV}^2 &= \Gamma^{\text{inv}}(h \rightarrow VV) \frac{512 \pi m_V^4}{v^2 \beta_V m_h^3} \times \frac{1}{\left(1 - 4 \frac{m_V^2}{m_h^2} + 12 \frac{m_V^4}{m_h^4}\right)} \quad (4) \\ \sigma^{\text{SI}}(\text{V-N}) &= \Gamma^{\text{inv}}(h \rightarrow VV) \frac{512 \pi m_V^4}{v^2 \beta_V m_h^3} \times \frac{1}{\left(1 - 4 \frac{m_V^2}{m_h^2} + 12 \frac{m_V^4}{m_h^4}\right)} \frac{m_N^2 f_N^2}{16 \pi m_h^4 (m_V + m_N)^2} \\ \sigma^{\text{SI}}(\text{V-N}) &= \Gamma^{\text{inv}}(h \rightarrow VV) \frac{32 m_V^4}{v^2 \beta_V m_h^7 (m_V + m_N)^2} \times \frac{m_N^2 f_N^2}{\left(1 - 4 \frac{m_V^2}{m_h^2} + 12 \frac{m_V^4}{m_h^4}\right)} \\ \sigma^{\text{SI}}(\text{V-N}) &= 32 \mu_{Vp}^2 \Gamma_{\text{inv}}^{\text{H}} \frac{m_V^2 m_N^2 f_N^2}{v^2 \beta_V m_h^7} \quad (5) \end{aligned}$$

Using Equation 5 one can transform the limit on  $\mathcal{B}_{H \rightarrow \text{inv}}$  into the vector line interpretation as in the green hashed band in Figure 9 of Ref. [23]. That figure shows the ATLAS Run-1 upper limit at the 90% CL on the WIMP-nucleon scattering cross section in a Higgs portal model as a function of the mass of the dark-matter particle, for a scalar, Majorana fermion, or vector-boson WIMP. The wide band is due to the old  $f_N$  which has a big uncertainty. LHC interpreted VDM limit was claimed to be model-independent and better than limits from direct detection in the regime of  $m_V < \frac{m_H}{2}$ . However, it drew controversial attention which will be discussed in Section 2.3.

### 2.3 Objection on EFT, first UV model

In the EFT approach used in LHC Run-1 [23], the mass of the VDM was entered arbitrarily, which leads to a non-renormalisable Lagrangian and violation of unitarity Ref.[25]. For this reason, it is safer to consider a better framework, i.e. a simple UV completion with a dark Higgs sector that gives mass to the vector DM via spontaneous electroweak symmetry breaking (EWSB). The simplest renormalisable Lagrangian for the Higgs portal VDM in such a UV model is given by Ref.[25]:

$$\mathcal{L}_{VDM} = -\frac{1}{4}V_{\mu\nu}V^{\mu\nu} + D_\mu \Phi^\dagger D^\mu \Phi - \lambda_\Phi(\Phi^\dagger \Phi - \frac{\nu_\Phi^2}{2})^2 - \lambda_{\Phi H}(\Phi^\dagger \Phi - \frac{\nu_\Phi^2}{2})(H^\dagger H - \frac{\nu_H^2}{2}), \quad (6)$$

where  $\Phi$  is the dark Higgs field which generates a nonzero mass for the VDM through spontaneous  $U(1)_X$  breaking,  $D_\mu \Phi = (\partial_\mu + ig_X Q_\Phi V_\mu) \Phi$  and  $g_X$  is the coupling constant.

From the Lagrangian, one can derive the invisible branching fractions of the Higgs decay [25]:

$$\Gamma_{\text{inv}}^H = \frac{g_X^2}{32\pi} \frac{m_H^3}{m_V^2} \left(1 - 4\frac{m_V^2}{m_H^2} + 12\frac{m_V^4}{m_H^4}\right) \left(1 - 4\frac{m_V^2}{m_H^2}\right)^{1/2}, \quad (7)$$

And then, the spin independent cross section of dark matter particles scattering, can be expressed as follows [25]:

$$\sigma^{\text{SI}}(\text{V-N}) = \sigma_p^{\text{SI}} = \cos^4(\alpha) m_H^4 F(m_V, m_i, \nu) \times (\sigma_p^{\text{SI}})_{\text{EFT}}, \quad (8)$$

$$(\sigma_p^{\text{SI}})_{\text{EFT}} = \frac{\mathcal{B}_{H \rightarrow \text{inv}} \Gamma_H^{\text{SM}}}{1 - \mathcal{B}_{H \rightarrow \text{inv}}} \frac{32 m_r^2 m_V^2 (m_p / \nu_H)^2 f_p^2}{m_H^7 \beta_\nu \left(1 - 4\frac{m_V^2}{m_H^2} + 12\frac{m_V^4}{m_H^4}\right)}, \quad (9)$$

where  $m_V$ ,  $m_p$ ,  $m_h$ ,  $\beta_\nu$  and  $m_r$  are the same given Section 2.

$(\sigma_p^{\text{SI}})_{\text{EFT}}$  is the spin independent cross section for dark matter particles from the EFT approach used in LHC Run-1 [23]. We can see clearly now that in the case of a UV completion model, the cross section has at least two additional parameters, the mass of the second scalar boson which is mostly singlet-like, and the mixing angle  $\alpha$  between the SM Higgs and the singlet scalar boson.

We investigated how the cross section evolves for the choice of  $\alpha$  and for different scenarios for the dark Higgs mass  $m_2$  in the range  $[10^{-2}, 1000]$  GeV (see Figure 1). The resulting bound on  $\sigma_p^{\text{SI}}$

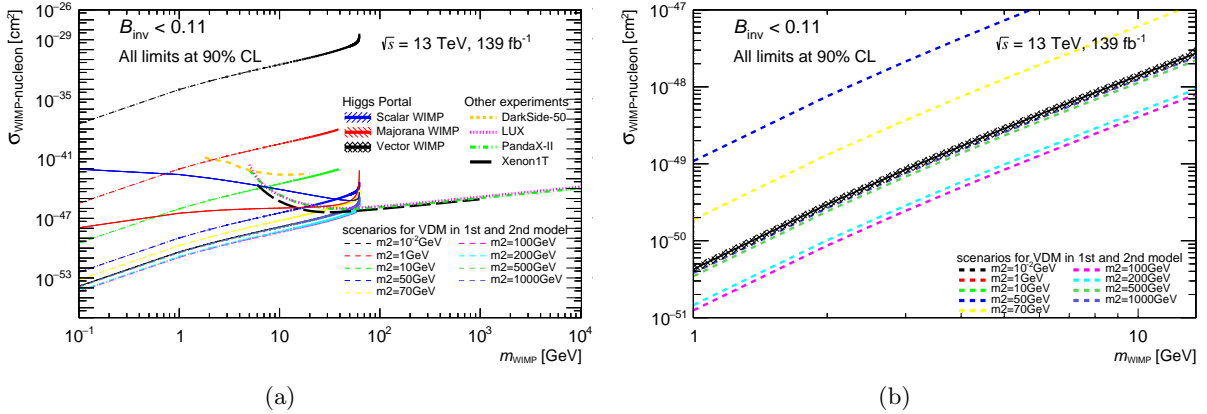


Figure 1:  $\sigma_p^{\text{SI}}$  as function of the mass of the VDM for the mixing angle  $\alpha = 0.2$ , and for the dark Higgs mass:  $10^{-2}$ , 1, 10, 5, 70, 1000, 500, 200, 100 GeV for dashed lines from top to bottom. Scalar, Majorana and the vector portals from EFT approach with other direct detection are depicted for comparison (see Figure 1(a)). In the right (Figure 1(b)) we zoomed around the EFT line to allow a clear comparison between different scenarios of dark Higgs mass and the EFT.

becomes weaker than the one based on EFT if the singlet-like scalar is lighter than the SM Higgs boson, and stronger if it is heavier than the SM Higgs boson. Also the UV model tends to coincide with EFT as the second scalar mass  $m_2$  get larger. The usual EFT approach applies only in the case of  $m_2 = m_h \cos(\alpha) / \sqrt{1 + \cos^2(\alpha)}$  or  $m_2 \rightarrow \infty$  and  $\alpha \rightarrow 0$ . and therefore the bounds on the  $\sigma_p^{\text{SI}}$  should be taken with caution.

## 2.4 Reanalyse EFT, second UV model

In Ref.[26], theorists reanalyse the possibility that a Higgs-portal with a vectorial dark matter state could represent a consistent EFT of its UV completion. A dark Higgs sector was introduced to reproduce the vector mass via spontaneous electroweak symmetry breaking. Therefore the complete Lagrangian for dark matter phenomenology is [26]:

$$\mathcal{L} = \frac{1}{2}\tilde{g}M_V(H_2\cos(\theta) - H_1\sin(\theta))V_\mu V^\mu + \frac{1}{8}\tilde{g}^2(H_1^2\sin^2(\theta) - 2H_1H_2\sin(\theta)\cos(\theta)) + H_2^2\cos^2(\theta)V_\mu V^\mu, \quad (10)$$

where  $H_1$  is the 125 GeV SM-like Higgs boson,  $H_2$  is the additional DM scalar state and  $\tilde{g}$  the new gauge coupling.

From the Lagrangian one can derive the expression for  $\Gamma_{inv}$  and  $\sigma_p^{SI}$  [26].

$$(\Gamma_{inv}^H)_{U(1)} = \frac{\tilde{g}^2\sin^2(\theta)}{32\pi} \frac{M_{H_1}^3}{M_V^2} \beta_{VH_1}, \quad (11)$$

$$\sigma^{SI}(V-N) = (\sigma_p^{SI})_{U(1)} = 32\cos^2(\theta)\mu_{Vp}^2 \frac{M_V^2}{M_{H_1}^3} \frac{BR(H_1 \rightarrow VV)\Gamma_{H_1}^{tot}}{\beta_{VH_1}} \left(\frac{1}{M_{H_2}^2} - \frac{1}{M_{H_1}^2}\right)^2 \frac{m_p^2}{v^2} |f_p^2|, \quad (12)$$

where  $\beta_{VH}$ ,  $BR(H \rightarrow VV) \equiv \Gamma(H \rightarrow VV)/\Gamma_H^{tot}$  and  $\mu_{Vp}$  are the same as in Section 2. The  $\sigma_{SI}^p$  is different from the formula in Ref.[26]. The scale was corrected from 8 to 32 after discussions with the authors of Ref.[26].

The prediction for VDM using EFT approach can be obtained in the limit  $\cos^2(\theta)M_H^4(1/M_{H_2}^2 - 1/M_{H_1}^2)^2 \approx 1$  where  $\sin(\theta) \ll 1$  and  $M_{H_2} \gg M_{H_1} = M_H$ .

Similar to what was done for the first model, we investigated the results for the choice of a mixing angle  $\theta = 0.2$  and different scenarios for the mass of the second boson  $M_{H_2}$  in the range  $[10^{-2}, 1000]$  GeV(see Figure 2).

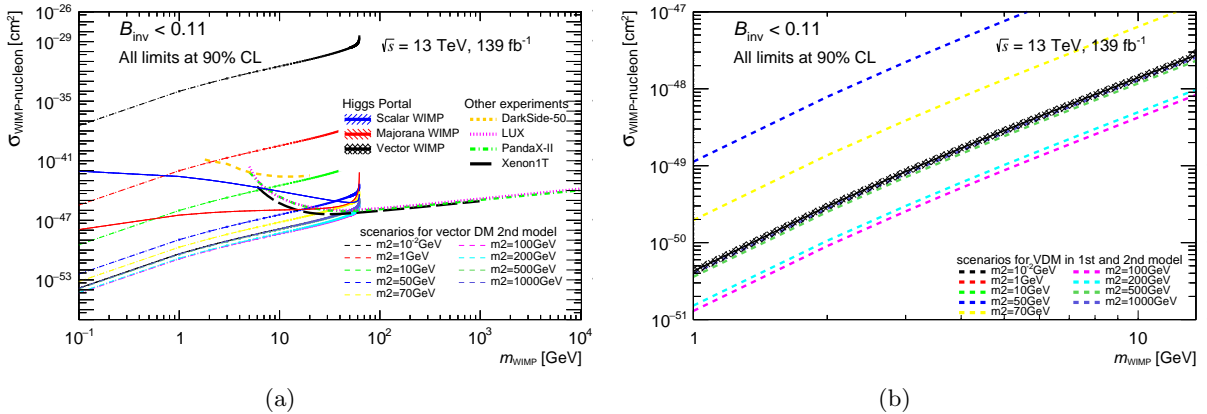


Figure 2:  $\sigma_p^{SI}$  as function of the mass of the vector dark matter(VDM) for the mixing angle  $\alpha = 0.2$ , and  $M_{H_2}=10^{-2}, 1, 10, 50, 100, 200, 500, 1000$  GeV. Scalar, Majorana and the vector portals from EFT approach with other direct detection are depicted for comparison(see Figure 2(a)). In the right (Figure 2(b)) we zoomed around the EFT line to allow a clear comparison between different scenarios of dark Higgs mass and the EFT.

This exercise is extremely important not only because it shows the difference between the EFT and its UV completion according to values of  $(\theta, m_2)$ , but also because it demonstrates that EFT approach could represent a viable limit of the renormalisable model in large region of its parameter space.

## 2.5 Radiative Higgs portal, third UV model

### 2.5.1 Lagrangian

This UV model [27] uses the same approach as introduced in other UV models mentioned in Sections 2.3 and 2.4. The vector DM is introduced as a gauge field of a  $U(1)'$  group which extends the SM symmetry; a Dark Higgs sector is added in to produce the vector boson mass via the Higgs spontaneous symmetry breaking mechanism. The Lagrangian of the vector part is as the following (Equation 2 of Ref. [27]):

$$\mathcal{L} \supset -\frac{1}{4}V_{\mu\nu}V^{\mu\nu} + (D_\mu\Phi)^\dagger(D^\mu\Phi) - V(\Phi) + \lambda_P|H|^2|\Phi|^2 \quad (13)$$

where  $\lambda_P$  is the mixing parameter between the SM Higgs boson and the dark Higgs mode of the field  $\Phi$ . This model has a distinctive feature in generating the hVV coupling, the fermions charged under  $SM \times U(1)'$  are added in, as shown below the fermionic part of the Lagrangian (Equation 4 of Ref. [27]):

$$\begin{aligned} \mathcal{L} \supset & -m\epsilon^{ab}(\psi_{1a}\chi_{1b} + \psi_{2a}\chi_{2b}) - m_n n_1 n_2 \\ & - y_\psi \epsilon^{ab}(\psi_{1a}H_b n_1 + \psi_{2a}H_b n_2) - y_\chi(\chi_1 H^* n_2 + \chi_2 H^* n_1) + h.c. \end{aligned} \quad (14)$$

where  $\psi, \chi, n$  are different fermion fields. That leads to loop induced hVV interaction as shown in Figure 3.

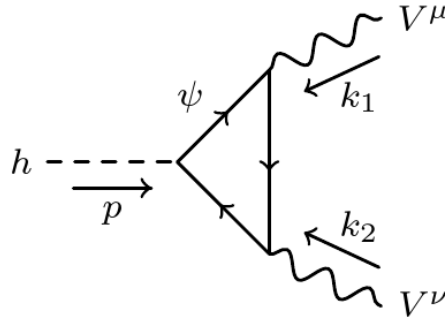


Figure 3: Fermion loop induced for hVV interaction. Figure 1 of Ref. [27]

### 2.5.2 Finding relation between $\sigma^{\text{SI}}(\text{V-N})$ and $\Gamma_{\text{inv}}^{\text{H}}$

There are many different scenarios for this UV model; the studied scenario in this note is the simplified case where the Higgs mixing parameter  $\lambda_P \ll 1$ , the charged fermions and the two heavier neutral states' masses are much heavier than the lightest neutral state mass, thus decouple from the Lagrangian. The minimal parameter space to be explored includes the vector mass  $m_V$ , the fermion mass  $m_f$ , the  $U(1)'$  coupling  $g$  and the Yukawa coupling  $y$  of the added fermion to the SM Higgs.

This model has no direct analytical relation between  $\Gamma_{\text{inv}}^{\text{H}}$  and  $\sigma^{\text{SI}}(\text{V-N})$ , their computations are extensive. To obtain upper limit of  $\sigma^{\text{SI}}(\text{V-N})$  versus  $m_{\text{V}}$  based on the upper limit on  $\mathcal{B}_{H \rightarrow \text{inv}}$ , one has to find values of  $(m_{\text{f}}, g, y)$  which satisfy the  $\mathcal{B}_{H \rightarrow \text{inv}}$  upper limit within a certain precision, then calculate  $\sigma^{\text{SI}}(\text{V-N})$ . In our calculation, the  $\mathcal{B}_{H \rightarrow \text{inv}}$  used is 11% at 90% CL from the recently published ATLAS VBF+MET analysis [28].

Explicitly, the task requires a scan through the set  $(m_{\text{f}}, g, y)$  for each  $m_{\text{V}}$  point to find values of  $\Gamma_{\text{inv}}^{\text{H}}$  corresponding to  $\mathcal{B}_{H \rightarrow \text{inv}}$  of 11% [28] within a relative precision of 1% to 0.1%. The choice of 0.1% to 1% precision is random; they are shown to have negligible impact on the results and the more stringent precision of 0.1% was chosen. Some parts of the phase space can be left out of the scan since there are other constraints on those parameters:

- $m_{\text{V}} < \frac{m_{\text{h}}}{2}$ , as for V being on-shell decay products of the Higgs boson.
- $m_{\text{f}} > \frac{m_{\text{h}}}{2}$ , to forbid the SM Higgs to decay to the additional fermions.
- $0 < g, y < 4\pi$ , as rule of thumb for dimensionless couplings satisfying perturbation.
- $0 < g^2 y < 40$ , a model constraint [27].

Two approaches in identifying the phase space are conducted. In the *first approach*, a single set of  $(m_{\text{f}}, g, y)$  for all  $m_{\text{V}}$  point is searched for, in order to get a single line of  $\sigma^{\text{SI}}(\text{V-N})$  vs  $m_{\text{V}}$ , similar to the EFT line shown in Figure 1 in Section 2.2. In the *second approach*, all satisfied  $(m_{\text{f}}, g, y)$  sets are used to construct a band of  $\sigma^{\text{SI}}(\text{V-N})$  vs  $m_{\text{V}}$ .

For both approaches, advocated by the nature of the model, different coarse to fine scanning steps of 0.1 to 0.01 on  $(g, y)$  are performed while keeping the same step of 1 GeV for  $m_{\text{V}}$  and 5 GeV for  $m_{\text{f}}$ , as shown in Table 1. Those are shown as follow; ultimately, the second approach is chosen while the former one fails.

Table 1: Scanning configurations for  $m_{\text{V}}$  and  $m_{\text{f}}$ , in context of the UV model in Ref. [27]

Variable	First bin	Last bin	Step
$m_{\text{V}}$ (GeV)	1	62	1
$m_{\text{f}}$ (GeV)	64	499	5

### Coarse scan

Scanning steps of 0.1 on  $(g, y)$  are performed while keeping the same step of 1 GeV for  $m_{\text{V}}$  and  $m_{\text{f}}$  as shown in Table 1. Detailed configurations for this scan can be found in Table 2. A relative precision of 0.1% on  $\Gamma_{\text{inv}}^{\text{H}}$  is required. The collected  $(m_{\text{f}}, g, y)$  after the scans are plotted as shown

Table 2: Scanning configurations in the coarse scan for  $g$  and  $y$  in the context of UV model in Ref. [27].

Variable	First bin	Last bin	Step
$g$	0	12	0.1
$y$	0	12	0.1

in Figure 4 in order to perform the first approach. However, none of them satisfy the full  $m_{\text{V}}$  range,

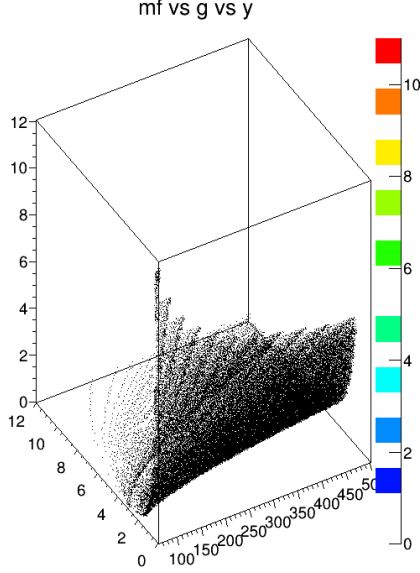


Figure 4: All the values of  $(m_f, g, y)$  satisfying  $\mathcal{B}_{H \rightarrow \text{inv}}$  of 11% with the relative precision of 0.1%. The color axis shows how many times a certain combination of  $(m_f, g, y)$  repeated. The color scale stops at 11, meaning that some of the combinations are not there for all the  $m_V$  points from 1 to 62 GeV.

so the finer scanning step in  $(g, y)$  and relaxation on the  $\Gamma_{\text{inv}}^H$  is performed next.

#### Fine scan

Scanning steps of 0.01 on  $(g, y)$  are performed while keeping the same step of 1 GeV for  $m_V$  and 5 GeV for  $m_f$  as shown in Table 1. Detailed configurations for this scan can be found in Table 3. A relative precision of 1% on  $\Gamma_{\text{inv}}^H$  is required.

Table 3: Scanning configurations in the coarse scan for  $g$  and  $y$  in the context of the UV model in Ref. [27].

Variable	First bin	Last bin	Step
$g$	0	12	0.01
$y$	0	12	0.01

After performing the two scans and trying the first approach to find a single set of  $(m_f, g, y)$ , none of the sets is found for all  $m_V$  in the range from 1 to 62 GeV. Furthermore, fixing  $m_f, g, y$  and scanning  $m_V$ , the  $\Gamma_{\text{inv}}^H$  varies by more than 74% from the lowest  $m_V$  to the highest  $m_V$  as shown in Figure 5. This makes it impossible to have all  $\Gamma_{\text{inv}}^H$  to be within  $\mathcal{B}_{H \rightarrow \text{inv}}$  with a precision of  $\sim 1\%$ . Therefore the first approach fails. The second approach is then used: all the found  $(m_f, g, y)$  for each  $m_V$  point are used to calculate  $\sigma^{\text{SI}}(\text{V-N})$ . The cross section values are then sorted from lowest to highest for each  $m_V$  point and plotted in Figure 6. The second approach succeeded in plotting  $\sigma^{\text{SI}}(\text{V-N})$  vs  $m_V$ . Discussion about the plots is presented in the next section.



#mf	g	y		
#65	10.37	0.01		
our invisible Higgs width= 11%/(1-0.011)*0.004 = 0.00049 GeV				
mv	mf	g	y	Higgs invisible width
1	65.0	10.37	0.001	7.44e-04
2	65.0	10.37	0.001	7.44e-04
3	65.0	10.37	0.001	7.43e-04
4	65.0	10.37	0.001	7.41e-04
5	65.0	10.37	0.001	7.39e-04
6	65.0	10.37	0.001	7.37e-04
7	65.0	10.37	0.001	7.35e-04
8	65.0	10.37	0.001	7.32e-04
9	65.0	10.37	0.001	7.28e-04
10	65.0	10.37	0.001	7.25e-04
11	65.0	10.37	0.001	7.20e-04
12	65.0	10.37	0.001	7.16e-04
13	65.0	10.37	0.001	7.11e-04
14	65.0	10.37	0.001	7.06e-04
15	65.0	10.37	0.001	7.00e-04
16	65.0	10.37	0.001	6.94e-04
17	65.0	10.37	0.001	6.88e-04
18	65.0	10.37	0.001	6.81e-04
19	65.0	10.37	0.001	6.75e-04
20	65.0	10.37	0.001	6.67e-04
21	65.0	10.37	0.001	6.60e-04
22	65.0	10.37	0.001	6.52e-04
23	65.0	10.37	0.001	6.44e-04
24	65.0	10.37	0.001	6.36e-04
25	65.0	10.37	0.001	6.28e-04
26	65.0	10.37	0.001	6.19e-04
27	65.0	10.37	0.001	6.10e-04
28	65.0	10.37	0.001	6.02e-04
29	65.0	10.37	0.001	5.93e-04
30	65.0	10.37	0.001	5.84e-04
31	65.0	10.37	0.001	5.75e-04
32	65.0	10.37	0.001	5.66e-04
33	65.0	10.37	0.001	5.58e-04
34	65.0	10.37	0.001	5.49e-04
35	65.0	10.37	0.001	5.41e-04
36	65.0	10.37	0.001	5.33e-04
37	65.0	10.37	0.001	5.25e-04
38	65.0	10.37	0.001	5.18e-04
39	65.0	10.37	0.001	5.11e-04
40	65.0	10.37	0.001	5.05e-04
41	65.0	10.37	0.001	5.00e-04
42	65.0	10.37	0.001	4.95e-04
43	65.0	10.37	0.001	4.91e-04
44	65.0	10.37	0.001	4.88e-04
45	65.0	10.37	0.001	4.86e-04
46	65.0	10.37	0.001	4.85e-04
47	65.0	10.37	0.001	4.85e-04
48	65.0	10.37	0.001	4.86e-04
49	65.0	10.37	0.001	4.88e-04
50	65.0	10.37	0.001	4.92e-04
51	65.0	10.37	0.001	4.97e-04
52	65.0	10.37	0.001	5.03e-04
53	65.0	10.37	0.001	5.10e-04
54	65.0	10.37	0.001	5.18e-04
55	65.0	10.37	0.001	5.25e-04
56	65.0	10.37	0.001	5.31e-04
57	65.0	10.37	0.001	5.35e-04
58	65.0	10.37	0.001	5.33e-04
59	65.0	10.37	0.001	5.21e-04
60	65.0	10.37	0.001	4.91e-04
61	65.0	10.37	0.001	4.27e-04

Figure 5: Fixing  $(m_f, g, y)$  and scanning through  $m_V$  for the UV model in Ref. [27].  $\Gamma_{\text{inv}}^H$  varies by more than 74% from the lowest  $m_V$  to the highest  $m_V$  value, thus makes it impossible to have all  $\Gamma_{\text{inv}}^H$  to be within  $\mathcal{B}_{H \rightarrow \text{inv}}$  with a precision of 1% or similar order of precision.

### 2.5.3 Results

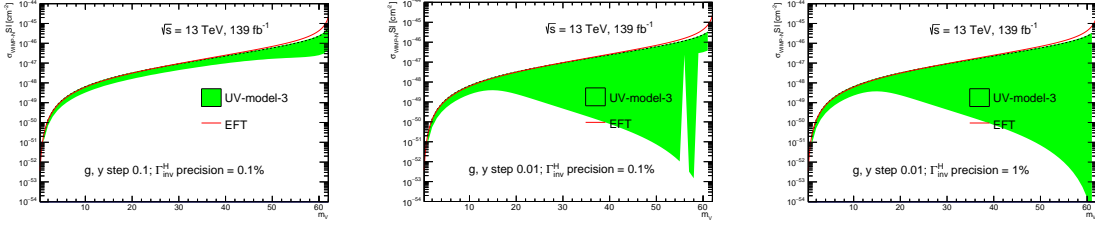


Figure 6: Green bands of upper limit on  $\sigma^{\text{SI}}(\text{V-N})$  from a coarse scan (left), fine scan (middle), fine scan with looser precision of  $\Gamma_{\text{inv}}^H$  (right) on  $(m_\chi, g, y)$  are shown in comparison with EFT red line, for the UV model in Ref. [27].

Figures 6 and 7 show that the precision on  $\Gamma_{\text{inv}}^H$  do not affect the upper bound on the  $\sigma^{\text{SI}}(\text{V-N})$  as the dashed lines remain the same for all cases, and stay very close to the EFT limit. However, as seen in the second and third plots of Figure 6, the fine scanning of  $(g, y)$  extends the lower bound of the green bands meaning that going finer in  $(g, y)$  one can achieve much better limits on  $\sigma^{\text{SI}}(\text{V-N})$  compared to EFT limit.

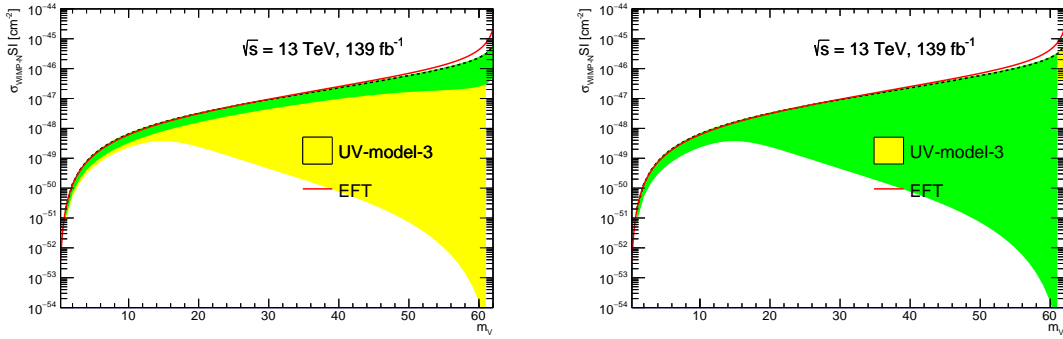


Figure 7: Superimposition of the interpretations for a coarse scan on top of a fine scan (left) and vice versa (right), for the UV model in Ref. [27].

## 3 Proposal

In this section we present our proposal of the Higgs portal VDM interpretation of the spin-independent dark-matter nucleon elastic scattering cross section using the invisible Higgs decay width. This proposal is motivated by the results presented in Section 2 and could be split in three parts.

Firstly, The limitations to the use of EFT approach as violation of unitarity and non-renormalisable Lagrangian (claimed in Section 2.3) is refuted by the recent review which derived the EFT Lagrangian from a certain UV model as shown in Section 2.4.

Secondly, presentation of the first and second UV models lines into the DM overlay plot. Sections 2.3 and 2.4 covered the performed study of these UV models: Using the mentioned first and second models the UV lines range for many different orders of magnitude, and the EFT approach limit is a special case for both of them. The most convenient way is to present the worst-best case scenarios for each of the two UV models.

Thirdly, introduction of the upper bound line as the third UV model representative limit. As illustrated in Section 2.5 the sensitivity of the third UV model shows that the bands of  $\sigma^{\text{SI}}(\text{V-N})$  vs  $m_V$  are better than the EFT approach limit. They also have the same consistent upper bound throughout different scanning configurations (arithmetic calculations also show only around 0.1% relative difference), and stay very close to the limit using the EFT approach. This third proposal is motivated in addition by the fact that we are interested in an upper limit.

Our proposals are shown in Figures 8, and 9, i.e. The interpretation of the radiative Higgs portal (third UV model) compared with EFT limit and with the first or second UV model correspondingly. Figures 9(a) and 9(b) show that the worst and best limits in the  $M_{H_2}$  range of  $[10^{-2}, 1000]$  GeV for both the first and the second UV models are similar.

After all considerations, the single final plot to be proposed is with the UV third model line, the EFT line, together with the first and second model worst-best lines merged as shown in Figure 10.

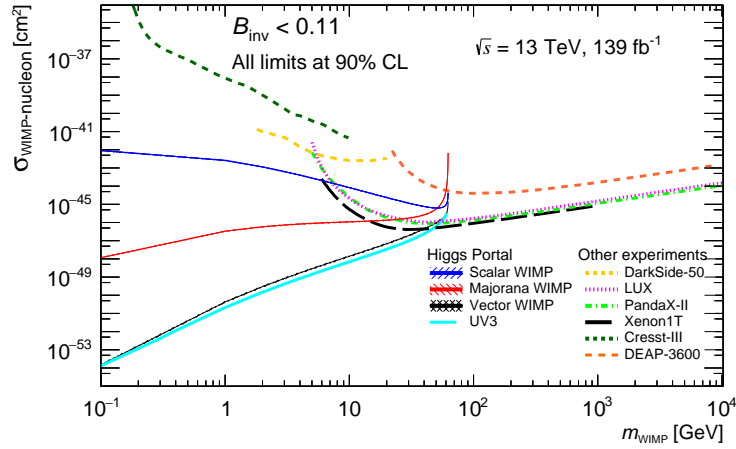


Figure 8:  $\sigma^{\text{SI}}(\text{V-N})$  limits from the radiative Higgs portal model (see Section 2.5) dubbed UV3 in the legend, compared to EFT limit in the DM overlay plot. As mentioned above, for UV3 we are on the scenario of small Higgs mixing parameter and one of the neutral fermions is much lighter than both the other two neutral states and both of the charged ones.

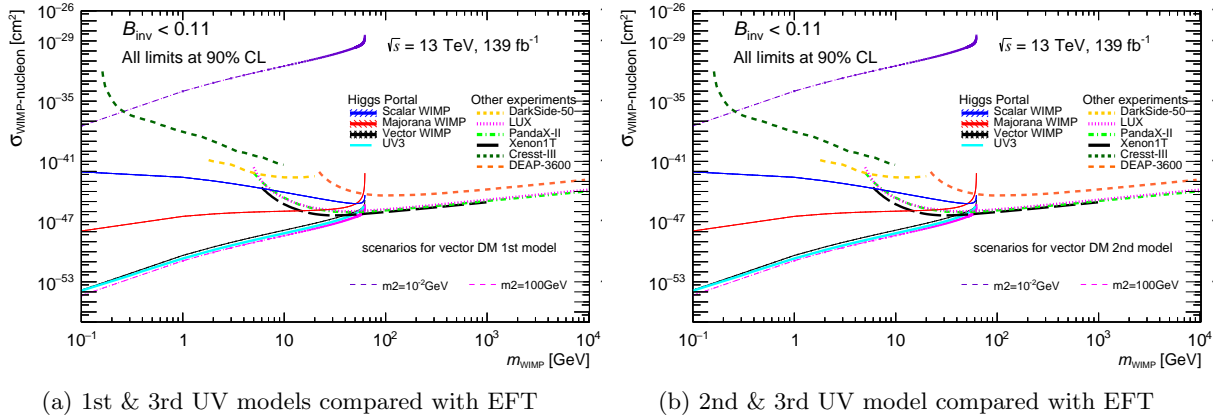


Figure 9:  $\sigma^{\text{SI}}(\text{V-N})$  limits from EFT approach compared with the radiative Higgs portal (see Section 2.5) and with (a) the first UV model (see Section 2.3), (b) the second UV model (see Section 2.4).

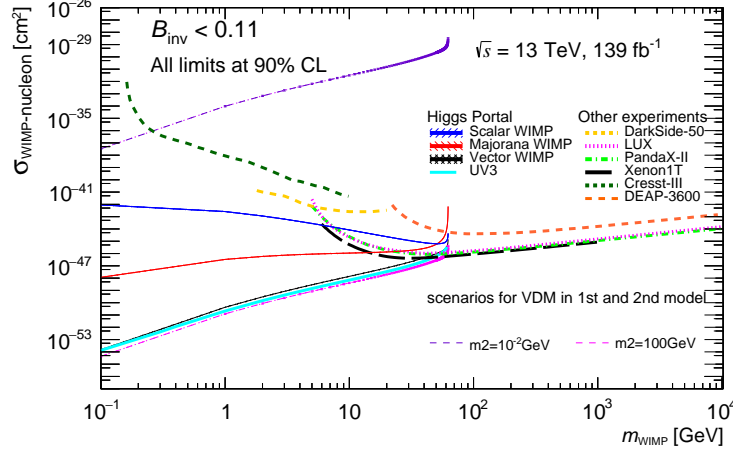


Figure 10:  $\sigma^{\text{SI}}(\text{V-N})$  limits from the radiative Higgs portal (see Section 2.5) compared to the first and second UV model (see Sections 2.3, 2.4) and EFT limit in the DM overlay plot. This is the final presenting proposal for VDM.

## 4 Sub-GeV WIMP mass

The LHC Higgs-portal DM interpretation of  $\sigma^{\text{SI}}(\text{WIMP-N})$  has been so far shown for  $m_V$  ranging from 1 GeV to  $\frac{m_H}{2}$ . The upper edge at  $\frac{m_H}{2}$  is for WIMP candidates to be produced on-shell from a Higgs decay. Whereas the lower edge at 1 GeV is arbitrarily coming from different concerns.

The first concern is about the theoretical or cosmological constraint on the WIMP mass. Particle Data Group 2019 review on DM shows the possibility of going to sub-GeV regime in many BSM models with WIMP paradigm [30]. Sections 26.6.2 and 26.6.3 of the PDG review discussed solid-state cryogenic detector experiment such as CRESST-III [31] which probes DM mass down to  $\sim 160$  MeV.

LHC Dark Matter Working Group (LHCDMWG) white paper [32] has recommendations for interpretation of simplified DM models which have s-channel spin-1 mediators decaying to fermions (invisible, aka DM candidates). To predict the relic density, the LHCDMWG recommends to work under the assumption that the DM annihilation cross section of the predicted models is fully responsible for the DM number density [32]. That leads to Figures 3 and 4 of Ref. [32] to have DM mass lower bound at few GeV. However, the mentioned bench mark models do not include Higgs portal scenario in which the scalar Higgs boson is the mediator.

The second concern is about the uncertainty on the  $\sigma^{\text{SI}}(\text{WIMP-N})$  calculation via a Higgs mediator for LHC interpretation in the WIMP sub-GeV mass regime. That calculation depends on the coupling of the Higgs boson to a single nucleon, first calculated in Ref. [33] and further improved in Ref. [29] whose  $f_N$  value of 0.38(18) is then used in Refs. [28, 34]. These calculations use lattice QCD calculations which are valid continuously from negative momentum transfer to positive momentum transfer, thus valid for 0-momentum transfer (our case of WIMP-nucleon elastic scattering).

Interactions with the main author of Ref. [29] also clears out our concern about  $f_N$  vs sub-GeV mass. In conclusion, the discussed two concerns above are not relevant for LHC Higgs-portal DM interpretation. Therefore, we propose to show in the DM overlay plot WIMP mass to sub-GeV domain, as low as 0.1 GeV to compare with 0.16 GeV as the lowest mass reached by CRESST-III [31].

## 5 Conclusion

Several approaches for the interpretation of  $\sigma^{\text{SI}}(\text{V-N})$  in Higgs-portal DM scenarios are presented. EFT approach is reviewed and shown to be safe to be reinserted in the DM overlay plot. Three UV models are studied, their results all are shown in different parameter phase spaces. In the first two UV models [25, 26], EFT is recovered when getting limits in certain region of their parameter phase spaces. Whereas for the third UV model [27], result in a simplified regime is better than the EFT approach limits. Therefore our final proposal for the DM overlay plot is to reinsert the EFT VDM line, include the upper bound of the third UV model, and the worst-best lines of the first and second UV models. Additionally, WIMP mass in the sub-GeV regime is discussed and proposed to be extended to 0.1 GeV in the DM overlay plot.

## References

- [1] D. Clowe et al., *A Direct Empirical Proof of the Existence of Dark Matter*, *The Astrophysical Journal* **648** (2006) L109, ISSN: 1538-4357, URL: <http://dx.doi.org/10.1086/508162> (cit. on p. 1).
- [2] J. L. Feng and J. Kumar, *The WIMPless Miracle: Dark-Matter Particles without Weak-Scale Masses or Weak Interactions*, *Phys. Rev. Lett.* **101** (2008) 231301, arXiv: 0803.4196 [hep-ph] (cit. on p. 1).
- [3] I. Antoniadis, M. Tuckmantel, and F. Zwirner, *Phenomenology of a leptonic goldstino and invisible Higgs boson decays*, *Nucl. Phys.* **B707** (2005) 215, arXiv: hep-ph/0410165 [hep-ph] (cit. on p. 1).
- [4] N. Arkani-Hamed, S. Dimopoulos, G. R. Dvali, and J. March-Russell, *Neutrino masses from large extra dimensions*, *Phys. Rev.* **D65** (2001) 024032, arXiv: hep-ph/9811448 [hep-ph] (cit. on p. 1).
- [5] A. Datta, K. Huitu, J. Laamanen, and B. Mukhopadhyaya, *Invisible Higgs in theories of large extra dimensions*, *Phys. Rev.* **D70** (2004) 075003, arXiv: hep-ph/0404056 [hep-ph] (cit. on p. 1).
- [6] S. Kanemura, S. Matsumoto, T. Nabeshima, and N. Okada, *Can WIMP Dark Matter overcome the Nightmare Scenario?*, *Phys. Rev.* **D82** (2010) 055026, arXiv: 1005.5651 [hep-ph] (cit. on p. 1).
- [7] A. Djouadi, O. Lebedev, Y. Mambrini, and J. Quevillon, *Implications of LHC searches for Higgs–portal dark matter*, *Phys. Lett. B* **709** (2012) 65, arXiv: 1112.3299 [hep-ph] (cit. on pp. 1–3).
- [8] A. Djouadi, A. Falkowski, Y. Mambrini, and J. Quevillon, *Direct Detection of Higgs-Portal Dark Matter at the LHC*, *Eur. Phys. J.* **C73** (2013) 2455, arXiv: 1205.3169 [hep-ph] (cit. on p. 1).
- [9] R. E. Shrock and M. Suzuki, *Invisible decays of Higgs bosons*, *Physics Letters B* **110** (1982) 250, ISSN: 0370-2693, URL: <http://www.sciencedirect.com/science/article/pii/0370269382912473> (cit. on p. 1).
- [10] D. Choudhury and D. P. Roy, *Signatures of an invisibly decaying Higgs particle at LHC*, *Phys. Lett.* **B322** (1994) 368, arXiv: hep-ph/9312347 [hep-ph] (cit. on p. 1).
- [11] O. J. P. Eboli and D. Zeppenfeld, *Observing an invisible Higgs boson*, *Phys. Lett.* **B495** (2000) 147, arXiv: hep-ph/0009158 [hep-ph] (cit. on p. 1).
- [12] H. Davoudiasl, T. Han, and H. E. Logan, *Discovering an invisibly decaying Higgs at hadron colliders*, *Phys. Rev.* **D71** (2005) 115007, arXiv: hep-ph/0412269 [hep-ph] (cit. on p. 1).
- [13] R. M. Godbole, M. Guchait, K. Mazumdar, S. Moretti, and D. P. Roy, *Search for ‘invisible’ Higgs signals at LHC via associated production with gauge bosons*, *Phys. Lett.* **B571** (2003) 184, arXiv: hep-ph/0304137 [hep-ph] (cit. on p. 1).
- [14] D. Ghosh, R. Godbole, M. Guchait, K. Mohan, and D. Sengupta, *Looking for an Invisible Higgs Signal at the LHC*, *Phys. Lett.* **B725** (2013) 344, arXiv: 1211.7015 [hep-ph] (cit. on p. 1).
- [15] G. Belanger, B. Dumont, U. Ellwanger, J. F. Gunion, and S. Kraml, *Status of invisible Higgs decays*, *Phys. Lett.* **B723** (2013) 340, arXiv: 1302.5694 [hep-ph] (cit. on p. 1).

- [16] D. Curtin et al., *Exotic decays of the 125 GeV Higgs boson*, *Phys. Rev. D* **90** (2014) 075004, arXiv: [1312.4992 \[hep-ph\]](#) (cit. on p. 1).
- [17] F. Petricca et al., “First results on low-mass dark matter from the CRESST-III experiment”, *15th International Conference on Topics in Astroparticle and Underground Physics (TAUP 2017) Sudbury, Ontario, Canada, July 24-28, 2017*, 2017, arXiv: [1711.07692 \[astro-ph.CO\]](#) (cit. on p. 1).
- [18] E. Behnke et al., *Final Results of the PICASSO Dark Matter Search Experiment*, *Astropart. Phys.* **90** (2017) 85, arXiv: [1611.01499 \[hep-ex\]](#) (cit. on p. 1).
- [19] D. S. Akerib et al., *Results from a search for dark matter in the complete LUX exposure*, *Phys. Rev. Lett.* **118** (2017) 021303, arXiv: [1608.07648 \[astro-ph.CO\]](#) (cit. on p. 1).
- [20] X. Cui et al., *Dark Matter Results From 54-Ton-Day Exposure of PandaX-II Experiment*, *Phys. Rev. Lett.* **119** (2017) 181302, arXiv: [1708.06917 \[astro-ph.CO\]](#) (cit. on p. 1).
- [21] E. Aprile et al., *Dark Matter Search Results from a One Ton-Year Exposure of XENON1T*, *Phys. Rev. Lett.* **121** (2018) 111302, arXiv: [1805.12562 \[astro-ph.CO\]](#) (cit. on p. 1).
- [22] P. Agnes et al., *Low-Mass Dark Matter Search with the DarkSide-50 Experiment*, *Phys. Rev. Lett.* **121** (2018) 081307, arXiv: [1802.06994 \[astro-ph.HE\]](#) (cit. on p. 1).
- [23] G. Aad et al., *Constraints on new phenomena via Higgs boson couplings and invisible decays with the ATLAS detector*, *JHEP* **11** (2015) 206, arXiv: [1509.00672 \[hep-ex\]](#) (cit. on pp. 1–4).
- [24] P. Calfayan, *Searches for invisible Higgs boson decays with ATLAS and CMS*, tech. rep., CERN, 2015, URL: <https://cds.cern.ch/record/2058131> (cit. on pp. 1, 2).
- [25] S. Baek, P. Ko, and W.-I. Park, *Invisible Higgs decay width vs. dark matter direct detection cross section in Higgs portal dark matter models*, *Physics Letters B* (2014), ISSN: 0370-2693, URL: <http://www.sciencedirect.com/science/article/pii/S0370269314006984> (cit. on pp. 2–4, 13).
- [26] G. Arcadi, A. Djouadi, and M. Kado, *The Higgs-portal for vector Dark Matter and the Effective Field Theory approach: a reappraisal*, *Phys. Lett. B* **805** (2020) 135427, arXiv: [2001.10750 \[hep-ph\]](#) (cit. on pp. 2, 5, 13).
- [27] A. DiFranzo, P. J. Fox, and T. M. P. Tait, *Vector Dark Matter through a Radiative Higgs Portal*, *JHEP* **04** (2016) 135, arXiv: [1512.06853 \[hep-ph\]](#) (cit. on pp. 2, 6–10, 13).
- [28] *Search for invisible Higgs boson decays with vector boson fusion signatures with the ATLAS detector using an integrated luminosity of 139 fb<sup>-1</sup>*, tech. rep. ATLAS-CONF-2020-008, CERN, 2020, URL: <http://cds.cern.ch/record/2715447> (cit. on pp. 2, 7, 12).
- [29] M. Hoferichter, P. Klos, J. Menéndez, and A. Schwenk, *Improved limits for Higgs-portal dark matter from LHC searches*, *Phys. Rev. Lett.* **119** (2017) 181803, arXiv: [1708.02245 \[hep-ph\]](#) (cit. on pp. 2, 12).
- [30] 2. PdG, M. Tanabashi et al. (Particle Data Group), *Phys. Rev. D* **98**, 030001 (2018) and 2019 update., tech. rep., 2019, URL: <https://pdg.lbl.gov/2019/reviews/rpp2019-rev-dark-matter.pdf> (cit. on p. 12).
- [31] A. Abdelhameed et al., *First results from the CRESST-III low-mass dark matter program*, *Phys. Rev. D* **100** (2019) 102002, arXiv: [1904.00498 \[astro-ph.CO\]](#) (cit. on p. 12).

- [32] A. Albert et al., *Recommendations of the LHC Dark Matter Working Group: Comparing LHC searches for dark matter mediators in visible and invisible decay channels and calculations of the thermal relic density*, *Physics of the Dark Universe* **26** (2019) 100377, ISSN: 2212-6864, URL: <http://www.sciencedirect.com/science/article/pii/S2212686419301682> (cit. on p. 12).
- [33] M. Shifman, A. Vainshtein, and V. Zakharov, *Remarks on Higgs-boson interactions with nucleons*, *Physics Letters B* **78** (1978) 443, ISSN: 0370-2693, URL: <http://www.sciencedirect.com/science/article/pii/0370269378904811> (cit. on p. 12).
- [34] ATLAS Collaboration, *Combination of searches for invisible Higgs boson decays with the ATLAS experiment*, *Phys. Rev. Lett.* **122** (2019) 231801, arXiv: 1904.05105 [hep-ex] (cit. on p. 12).